

# The Higgs mass in the MSSM infrared fixed point scenario\*

J.A. Casas <sup>¶</sup>, J.R. Espinosa <sup>†</sup> and H.E. Haber <sup>§</sup>

<sup>¶</sup> Instituto de Estructura de la Materia, CSIC  
Serrano 123, 28006 Madrid, Spain  
casas@cc.csic.es

<sup>†</sup> CERN, TH Division

CH-1211 Geneva 23, Switzerland  
espinosa@mail.cern.ch

<sup>§</sup> Santa Cruz Institute for Particle Physics  
University of California, Santa Cruz, CA 95064, USA  
haber@scipp.ucsc.edu

## Abstract

In the infrared fixed point scenario of the minimal supersymmetric model (MSSM), the top-quark mass and other physical quantities of the low-energy theory are insensitive to the values of the parameters of the theory at some high energy scale. In this framework we evaluate the light CP-even Higgs mass,  $m_{h^0}$ , taking into account some important effects that had not been previously considered. The most notable of these is the supersymmetric correction to the relation between the running and the physical top-quark masses, which lowers the value of  $\tan \beta$ . As a result, the predicted value of  $m_{h^0}$  is significantly lower than in previous evaluations. Assuming a supersymmetric threshold  $M_S \leq 1$  TeV, we find an absolute upper bound of  $m_{h^0} \leq 97 \pm 2$  GeV; the most plausible value of  $m_{h^0}$  lies somewhat below the upper bound. This places the Higgs boson well within the reach of the LEP-2 Higgs search.

CERN-TH/98-12  
January 1998

---

\*Research supported in part by: the CICYT, under contract AEN95-0195 (JAC); the European Union, under contract CHRX-CT92-0004 (JAC); and the U.S. Department of Energy, grant DE-FG03-92ER40689.

# 1 Introduction

Models of low-energy supersymmetry can add many new parameters to the Standard Model. The minimal supersymmetric extension of the Standard Model (MSSM) is minimal only in its choice of particle content. The number of free parameters of the model is quite large unless additional theoretical assumptions are imposed. The parameter freedom of the MSSM is due mostly to soft supersymmetry-breaking parameters, whose theoretical origins are presently unknown. It is common practice to treat the parameters of the MSSM as running parameters and impose a particular structure on the soft supersymmetry breaking terms at a common high energy scale [such as the Planck scale ( $M_P$ ) or grand unification (GUT) scale ( $M_X$ )]. Using the renormalization group equations (RGEs), one can then derive the values of the low-energy MSSM parameters.

A particularly attractive framework, which we will adopt in this paper, consists of assuming universality of soft-breaking parameters at the high-energy unifying scale. Universality is a desirable property not only to reduce the number of independent model parameters, but also to avoid unsuppressed flavor changing neutral currents (FCNCs) [1]. Universality of scalar and gaugino mass parameters in the high energy theory is an automatic consequence of the *minimal* supergravity (SUGRA) framework [2] and approximately holds in several string-derived SUGRA scenarios [3].

The resulting low-energy supersymmetric theory that emerges depends on five supersymmetric model parameters: a common scalar mass,  $m$ , a common gaugino mass,  $M$ , a common flavor-diagonal trilinear scalar coupling,  $A$ , a supersymmetric Higgs mass parameter  $\mu$ , and an off-diagonal Higgs squared-mass parameter  $m_{12}^2$  (often called  $B\mu$ ). These parameters are high-energy scale parameters (defined at either  $M_X$  or  $M_P$ ) and serve as initial conditions for the RGEs. Electroweak symmetry breaking in the low-energy theory is radiatively generated when one of the Higgs squared-masses is driven negative by renormalization group (RG) running. Then, by imposing the minimum conditions for the Higgs potential, one can eliminate  $\mu^2$  and  $m_{12}^2$  in favor of the electroweak symmetry breaking scale,  $v^2 \equiv v_1^2 + v_2^2 \simeq (174 \text{ GeV})^2$ , and  $\tan\beta \equiv v_2/v_1$ , where,  $v_1$  and  $v_2$  are the Higgs vacuum expectation values. The sign of  $\mu$  is not fixed in this procedure, and remains a free parameter.

Clearly, the previously described SUGRA theory is a highly constrained version of the MSSM. Nevertheless, there can be additional interesting constraints. In particular, one sometimes finds that certain low-energy MSSM parameters are very insensitive to the initial high energy values of the SUGRA parameters. Such a possibility is very exciting, since it allows one to potentially understand the physical value of some low-energy parameters without a detailed knowledge of the physics at high energies.

The classic example of the scenario just described is the quasi-infrared fixed point (IFP) prediction for the top-quark Yukawa coupling [4,5,6,7,8,9,10,11,12,13,14]<sup>1</sup>. As is

---

<sup>1</sup>The quasi-infrared fixed point differs from the infrared fixed point of Pendleton and Ross (PR)[15]. The PR-fixed point is an infrared stable fixed point that is reached at a scale  $Q$  for sufficiently large  $M_X/Q$ . However, in practice  $M_X/m_Z$  is not large enough, so the PR-fixed point solution does not govern the low-energy value of the top-quark Yukawa coupling. On the other hand, it follows from eqs. (1)–(3) that the top-quark Yukawa coupling is driven to the quasi-infrared fixed point as long as  $Y_t(0)F(t_Z) \gg 1/6$ , where  $t_Z \equiv \ln(M_X^2/m_Z^2)$ .

well known [5], the one-loop RGE of the top-quark Yukawa coupling,  $Y_t \equiv h_t^2/(4\pi)^2$ , can be integrated analytically for moderate values of  $\tan\beta \sim \mathcal{O}(1)$ :

$$Y_t(t) = \frac{Y_t(0)E(t)}{1 + 6Y_t(0)F(t)} \quad (1)$$

with

$$E(t) = (1 + \beta_3 t)^{16/3b_3} (1 + \beta_2 t)^{3/b_2} (1 + \beta_1 t)^{13/9b_1}, \quad F(t) = \int_0^t E(t') dt'. \quad (2)$$

In eq. (2),  $\beta_i = \alpha_i(0)b_i/4\pi$  are the one-loop beta functions of the gauge couplings  $\alpha_i(t)$ , with  $(b_1, b_2, b_3) = (11, 1, -3)$ , and  $t = \ln(M_X^2/Q^2)$ , where  $Q$  is the renormalization scale. This one-loop behavior leads to the existence of the quasi-infrared fixed point. Namely, for  $Y_t(0) \rightarrow \infty$ ,

$$Y_t(t) \rightarrow Y_f(t) \equiv \frac{E(t)}{6F(t)}. \quad (3)$$

Numerically, one finds that  $Y_t$  at the electroweak scale differs negligibly from  $Y_f$  for a wide range of  $Y_t(0) \gtrsim 0.01$ , so in this sense the low-energy value of  $Y_t$  is indeed insensitive to its high-energy value  $Y_t(0)$ . The value of the top-quark mass depends both on the low-energy values of  $Y_t$  and  $\tan\beta$ , so at this stage we do not have a prediction for the top-quark mass. Nevertheless, the parameter freedom has been reduced, since given the top-quark mass,  $\tan\beta$  is now predicted. Actually,  $\tan\beta$  typically turns out to be near 1, in which case the previous derivation is fully justified<sup>2</sup>.

In this paper, we focus on the prediction of the light CP-even Higgs mass ( $m_{h^0}$ ) in the IFP scenario as a function of the minimal SUGRA parameters. We improve on previous work in the literature by taking into account a number of effects not fully considered in previous works. These include: corrections to  $\tan\beta$  due to supersymmetric thresholds; evolution of  $\tan\beta$  from the electroweak scale to the supersymmetry-breaking scale; and a precise evaluation of radiative electroweak breaking and the top-squark (stop) mixing parameter. All these effects have a significant impact on the value of  $m_{h^0}$ . In addition, we have computed  $m_{h^0}$  using the most refined methods available, including subdominant contributions and corrections from stop non-degeneracy. This substantially reduces the theoretical uncertainty of our results with respect to previous literature. Our final result on the upper bound on the Higgs mass is about 10 GeV smaller than in previous evaluations. This is substantial decrease, which has important implications for the LEP-2 search.

In Section 2, we discuss the IFP scenario and the calculation of  $\tan\beta$ , as well as the stop mixing parameter, including all the new effects mentioned above. We address a number of effects not previously considered which can significantly affect the predicted value of  $\tan\beta$  and the Higgs mass. In Section 3, we review the dependence of the Higgs mass on the supersymmetric parameters. In Section 4, we explore the consequences of

---

<sup>2</sup> If one solves the complete set of RGEs for the top and bottom-quark Yukawa couplings, one finds another IFP solution with  $\tan\beta \sim m_t/m_b$ . In this paper, we will not address this large  $\tan\beta$  scenario since, in the minimal SUGRA approach described above, it requires a precise (unnatural) fine-tuning of high-energy parameters in order to ensure the correct radiative electroweak symmetry breaking [16].

the IFP scenario for the predicted value of the Higgs mass, giving full numerical results and comparing to the previous literature. Conclusions are presented in Section 5.

## 2 The IFP scenario revisited

In Section 1, we reviewed the quasi-infrared fixed point (IFP) scenario in which the low-energy value of the top-quark Higgs Yukawa coupling is driven to a quasi-infrared fixed point value,  $Y_f$ . Formally, this limit is derived by taking  $Y_t(0) \rightarrow \infty$ . This is not theoretically consistent as it stands, since the derivation given above was based on a one-loop RGE, while large values of  $Y_t(0)$  clearly lie outside the perturbative regime. However, it has been shown [17] that the domain of attraction of the quasi-IFP is large and accurately represented by the one-loop approximation. In particular,  $Y_t(0)$  rapidly approaches  $Y_f$ , even for values of  $Y_t(0)$  still in the perturbative region. This allows one to consider the IFP limit as a meaningful physical possibility. For example, starting with  $Y_t(0) = 0.1$  the one-loop value of  $Y_t(t)$  at the weak scale differs from  $Y_f$  by 0.27%. In this paper, we employ two-loop RGE's for the evolution of the gauge and Yukawa couplings. For definiteness, we choose  $Y_t(0) = 0.1$ , although the results are insensitive to this choice as argued above.

Another subtlety concerning the precise definition of the IFP scenario is the choice of the unification scale,  $M_X$ , and  $\alpha_i(0)$ . Here, we follow the approach of Ref. [18]. First, we take the experimental values of  $\alpha_i(Q = m_Z)$  as input parameters and evaluate the corresponding supersymmetric  $\overline{\text{DR}}$  values,  $\hat{\alpha}_i(m_Z)$ , taking into account all the supersymmetric threshold corrections<sup>3</sup> [the  $\hat{\alpha}_i(m_Z)$  do not have a direct physical meaning; see Ref. [18] for more details]. Then, the two-loop running of  $\hat{\alpha}_1(t)$ ,  $\hat{\alpha}_2(t)$  to high scales defines a unification scale  $M_X$  and a “unified” coupling constant  $\hat{\alpha}(0)$ . Finally, the running of  $\hat{\alpha}_3$  from  $m_Z$  to  $M_X$  gives the value of  $\hat{\alpha}_3(0)$ . In general, the latter does not coincide (even within the error bars) with  $\hat{\alpha}(0)$ , although the difference is small and can be attributed to, *e.g.*, threshold corrections either from a GUT or stringy origin.

The IFP scenario defined in the context of the SUGRA approach depends on additional parameters  $m$ ,  $M$ ,  $A$ ,  $\tan\beta$  and  $\text{sign}(\mu)$  as described in Section 1. However, the subset of independent parameters is substantially smaller. In the IFP scenario, the low-energy value of  $A_t$  (the trilinear scalar coupling of the Higgs boson and stops) is also driven to an infrared quasi-fixed point. At the one-loop level

$$A_t(t) \rightarrow M \left[ \frac{1}{4\pi} \left( \frac{16}{3} \alpha_3(0) h_3 + 3 \alpha_2(0) h_2 + \frac{13}{9} \alpha_1(0) h_3 \right) - t \frac{E(t)}{F(t)} + 1 \right], \quad (4)$$

where  $h_i(t) = t/(1 + \beta_i t)$ . Therefore the value of  $A(0)$  in the IFP limit is irrelevant. Although this is not true for the remaining trilinear couplings  $A_b, A_\tau$ , *etc.*, the latter  $A$ -parameters have a negligible effect in the determination of the Higgs mass, which is the main goal of this paper. The value of  $\tan\beta$ , evaluated at the scale  $Q = M_t$  (where

---

<sup>3</sup>Of course, these threshold corrections depend on the values of supersymmetric masses and thus on the remaining independent parameters of the model.

$M_t$  is the physical top-quark mass), is determined by using

$$v_2(M_t) = \frac{m_t(M_t)}{4\pi\sqrt{Y_t(M_t)}}, \quad (5)$$

and the approximate  $\overline{\text{DR}}$  relation [18]

$$v(m_Z) \simeq \left[ 175.8 + 0.32 \ln \left( \frac{m^2 + 4M^2}{m_Z^2} \right) \right] \text{ GeV}. \quad (6)$$

The distinction between the physical top-quark mass,  $M_t$ , and the running top-quark mass,  $m_t(M_t)$ , should not be ignored. Explicitly, the physical top-quark mass is given by

$$M_t = m_t(M_t) \left[ 1 + \frac{\Delta m_t}{m_t} \right], \quad (7)$$

where the one-loop correction,  $\Delta m_t$ , receives two important contributions: the well-known QCD gluon correction<sup>4</sup>

$$\left( \frac{\Delta m_t}{m_t} \right)_{\text{QCD}} = \frac{5g_3^2}{12\pi^2}, \quad (8)$$

and the stop/gluino correction [18,19]

$$\begin{aligned} \left( \frac{\Delta m_t}{m_t} \right)_{\text{SUSY}} = & -\frac{g_3^2}{12\pi^2} \left\{ B_1(m_t, M_{\tilde{g}}, m_{\tilde{t}_1}) + B_1(m_t, M_{\tilde{g}}, m_{\tilde{t}_2}) \right. \\ & \left. - \sin(2\theta_t) \frac{M_{\tilde{g}}}{m_t} [B_0(m_t, M_{\tilde{g}}, m_{\tilde{t}_1}) - B_0(m_t, M_{\tilde{g}}, m_{\tilde{t}_2})] \right\}, \end{aligned} \quad (9)$$

where  $\theta_t$  is the stop mixing angle,  $m_{\tilde{t}_1} > m_{\tilde{t}_2}$ , and

$$B_n(p; m_1, m_2) \equiv - \int_0^1 dx x^n \ln \left[ \frac{(1-x)m_1^2 + xm_2^2 - x(1-x)p^2}{m_t^2} \right]. \quad (10)$$

(We note that the Standard Model two-loop QCD correction [20] and the electroweak correction [21] are each of order 1% and almost cancel one another.) While the one-loop gluon correction [eq. (8)] yields a 6% relative top-quark mass shift, the supersymmetric correction in our scenario is of the same sign and can be as large as the gluon correction for  $M \gtrsim 500$  GeV. Note that the stop/gluino correction (which increases with the supersymmetric masses) is a consequence of working in the effective supersymmetric theory without decoupling the supersymmetric particles, as is usually done in the IFP literature when considering the running of  $Y_t$ . (In practice, this is the most convenient way to perform the analysis; for an alternative approach see Ref. [22].) However, the correction given by eq. (9) has never been included in the published analyses of the IFP scenario. This correction has the noteworthy effect of reducing the ratio  $m_t(M_t)/M_t$ , and consequently lowering the IFP value of  $\tan \beta$ . As a result, the predicted value for mass of the light CP-even Higgs boson is significantly reduced, as shown in Section 4.

---

<sup>4</sup>The factor 5 in eq. (8) in the  $\overline{\text{DR}}$  scheme should be replaced by 4 in the  $\overline{\text{MS}}$  scheme [18].

Let us turn now to the  $\mu$ -parameter. We noted in Section 1 that  $\mu$  can be determined (up to a sign) by imposing the condition of electroweak symmetry breaking and fixing the  $Z$  mass to its physical value. More precisely, from the minimization of the renormalization group improved tree-level Higgs potential, one gets

$$\mu^2 + \frac{1}{2}m_Z^2 = \frac{1}{\tan^2 \beta - 1} \left( m_{H_1}^2 - \tan^2 \beta m_{H_2}^2 \right), \quad (11)$$

where  $m_{H_1}^2, m_{H_2}^2$  are the low-energy values of the soft squared-masses of the  $H_1, H_2$  Higgs fields (subject to the condition  $m_{H_1}^2 = m_{H_2}^2 = m^2$  at  $Q = M_X$ ). It is important to note that the result given in eq. (11) is only accurate enough if the tree-level potential is evaluated at a scale where the radiative corrections are minimized. This essentially happens for a scale of order the stop masses [23,24]. From now on we will take that scale,  $M_S$ , as the average of the stop squared-mass eigenvalues

$$M_S^2 \equiv \frac{1}{2} \left( m_{t_1}^2 + m_{t_2}^2 \right). \quad (12)$$

Consequently, all the quantities appearing in eq. (11) (including  $\mu$  and  $m_Z$ ) are to be taken at  $Q = M_S$ .<sup>5</sup> From eq. (5), eq. (6) *plus* the renormalization group evolution of  $H_1, H_2$  with their anomalous dimensions, we can determine the value of  $\tan \beta$  at any scale using the corresponding RGE for  $\tan \beta$ :

$$\frac{d \tan \beta}{dt} \simeq \frac{3}{2} Y_t \tan \beta. \quad (13)$$

This result can be employed to determine the value of  $\tan \beta$  at  $M_S$ . The running of  $\tan \beta$  has been ignored in the IFP literature and produces significant corrections in the final results.

From eqs. (4)–(6) and eq. (11) it follows that the only relevant independent parameters for predicting the light CP-even Higgs mass,  $m_{h^0}$ , in the IFP scenario are  $m$  and  $M$ . The parameters  $m$  and  $M$  can be traded in for  $M_S$  and  $x \equiv M/m$ . Notice that in either case  $\text{sign}(\mu)$  may be absorbed, by a redefinition of fields, into the sign of  $M$  (or equivalently, the sign of  $x$ ). Besides the simplicity of this scenario, the fact that all the relevant low-energy quantities can be expressed in terms of  $M_S$  and  $x$  has important consequences for the prediction of the light CP-even Higgs mass. In particular, the mass splitting between stops and the effective mixing<sup>6</sup>

$$X_t \equiv A_t + \mu \cot \beta, \quad (14)$$

which play an important role in the computation of  $m_{h^0}$  (see Section 3) are no longer independent parameters, but are calculable quantities in terms of  $M_S$  and  $x$ . Since they cannot be simultaneously “tuned” to the values that maximize  $m_{h^0}$ , this produces an

---

<sup>5</sup>Even including the one-loop radiative corrections,  $\Delta V_1$ , to the tree-level potential,  $V_0$ , and using eq. (11) accordingly modified, is not in general a precise procedure since  $V_0 + \Delta V_1$  at  $Q = m_Z$  still yields inaccurate results if  $M_S^2 \gg m_Z^2$ , as it is normally the case [24] (see the comments at the end of the Appendix).

<sup>6</sup>The convention for the sign of  $\mu$  in eq. (14) is opposite the one employed in Ref. [25].

effective lowering of the upper bound on  $m_{h^0}$ . These issues will be carefully analyzed in the next two sections.

There is yet another source of additional constraints on the theory, namely the desirable absence of dangerous charge and color breaking (CCB) minima [26,27] or unbounded from below (UFB) directions [27] in the scalar potential. CCB and UFB constraints have been recently analyzed for the IFP scenario [28]. Since all the physics in which we are interested depends on just two parameters,  $M$  and  $m$  (or equivalently  $M_S$  and  $x$ ), we must focus on the CCB and UFB constraints involving these quantities. This means, in particular, that the CCB constraints involving the trilinear scalar couplings different from the top one, *i.e.*  $A_u, A_d, A_s$ , *etc.*, have no relevance to us since their low-energy values may be tuned at will by varying the initial high-energy parameter,  $A(0)$ . This is not the case for the low-energy top trilinear scalar coupling,  $A_t$ , which in our scenario is driven to an infrared fixed point given by eq. (4) [more generally, by eq. (32)], namely  $A_t \simeq -1.2M$ . This value, however, is well inside the region allowed by the CCB bounds [28]. On the other hand, UFB bounds strongly restrict the  $x \equiv M/m$  parameter [28] in the IFP scenario, namely the absence of UFB directions requires  $|x| \leq 1$ . In any case, the results presented in Section 4 imply that for  $x > 1$  the value of  $m_{h^0}$  hardly changes as a function of  $x$  (*i.e.*, it already reaches its large  $x$  asymptotic limit at  $x = 1$ ). Thus, in practice the CCB and UFB constraints do not restrict the bounds on  $m_{h^0}$  in the IFP scenario.

### 3 The MSSM Higgs mass

The Higgs sector of the MSSM consists of five physical states: two neutral CP-even scalars  $h^0$  and  $H^0$  (with  $m_{h^0} \leq m_{H^0}$ ), one neutral CP-odd scalar  $A^0$ , and a charged Higgs pair  $H^\pm$ . The quadratic terms of the Higgs potential consists of two diagonal squared-mass terms:  $m_i^2 \equiv m_{H_i}^2 + |\mu|^2$ , and one off-diagonal squared-mass term,  $m_{12}^2$ . When the minimum condition is imposed, the diagonal squared-mass terms are traded in for the vacuum expectation values  $v_1$  and  $v_2$ . Thus, the tree-level Higgs sector depends on only two new parameters:  $\tan\beta$  and  $m_{12}^2$ . It is convenient to replace  $m_{12}^2$  with the physical parameter  $m_{A^0}$ . Then, all other Higgs masses and couplings can be expressed at tree-level in terms of  $\tan\beta$  and  $m_{A^0}$ .

The prediction for the mass of the lightest CP-even neutral Higgs boson is of particular interest to the LEP Higgs search, since this Higgs scalar would be discovered first if it lies within the reach of the LEP-2 collider. In particular, the MSSM predicts that at tree-level,  $m_{h^0} \leq m_Z |\cos 2\beta| \leq m_Z$ . When radiative corrections are included, the light Higgs mass upper bound may be significantly increased above the tree-level prediction. This has profound effects on the LEP Higgs search. LEP-2 running at its maximum energy ( $\sqrt{s} \simeq 200$  GeV) and luminosity is expected to be sensitive to Higgs masses up to about 100 GeV [29]. Thus, the possibility of large radiative corrections to  $m_{h^0}$  implies that LEP cannot be sensitive to the full MSSM Higgs sector parameter space.

The mass of  $h^0$  can be calculated in terms of the two parameters of the Higgs sector mentioned above ( $m_{A^0}$  and  $\tan\beta$ ) and other MSSM soft-supersymmetry-breaking pa-

rameters that affect the Higgs mass through virtual loops [30,31,32,33,34,35,36,37,38,39]. The largest contribution to the one-loop radiative corrections is enhanced by a factor of  $m_t^4$  and grows logarithmically with the stop mass. Thus, higher order radiative corrections can be non-negligible for large stop masses, in which case the large logarithms must be resummed using renormalization group techniques [34,35,36,37,38,39].

For our numerical work, we will follow the simple analytic procedure for accurately approximating  $m_{h^0}$  described in Ref. [39], to which we refer the reader for details. Similar results are obtained using the alternative approximation of Refs. [37,38]. These analytic formulae incorporate both the leading one-loop and two-loop effects and the RG-improvement. Also included are the leading effects at one loop of the supersymmetric thresholds (the most important effects of this type are squark mixing effects in the third generation).

In the limit  $m_{A^0} \gg m_Z$ , which holds in the IFP scenario, only  $h^0$  remains light (with couplings nearly identical to those of the Standard Model Higgs boson), and its squared-mass including renormalization group improvement is given by a formula of the form<sup>7</sup> [39]

$$m_{h^0}^2 \simeq (m_{h^0}^2)_{\text{1LL}} [m_t(\mu_t)] + (\Delta m_{h^0}^2)_{\text{mix}} [m_t(\mu_{\tilde{t}})] , \quad (15)$$

where

$$\mu_t \equiv \sqrt{m_t M_S} , \quad \mu_{\tilde{t}} \equiv M_S . \quad (16)$$

In particular, the numerically integrated RG-improved CP-even Higgs mass is well approximated by replacing all occurrences of  $m_t$  in  $(m_{h^0}^2)_{\text{1LL}}$  and  $(\Delta m_{h^0}^2)_{\text{mix}}$  by the corresponding running masses evaluated at the judicious choice of scales indicated above.

The first term in eq. (15) is the one-loop leading logarithmic contribution to the squared-mass, given by

$$(m_{h^0}^2)_{\text{1LL}} \simeq m_Z^2 \cos^2 2\beta + \frac{g^2 N_c m_t^4(\mu_t)}{8\pi^2 m_W^2} \ln \left( \frac{m_{\tilde{t}_1} m_{\tilde{t}_2}}{m_t^2} \right) , \quad (17)$$

where  $\tan \beta$  is evaluated at  $m_Z$  and  $N_c = 3$ . Subdominant terms not written in eq. (17) can also be important for a precise determination of  $m_{h^0}$ . They can be found in Ref. [39] and were included in our numerical analysis. The second term in eq. (15) adds the important effects of stop mixing; and takes the form (again we display only the dominant terms)

$$(\Delta m_{h^0}^2)_{\text{mix}} \simeq \frac{g^2 N_c}{16\pi^2 m_W^2} m_t^4(\mu_{\tilde{t}}) \left\{ X_t^2 \left[ 2h(m_{\tilde{t}_1}^2, m_{\tilde{t}_2}^2) + X_t^2 g(m_{\tilde{t}_1}^2, m_{\tilde{t}_2}^2) \right] \right\} \quad (18)$$

where  $X_t$  is given by eq. (14), and

$$\begin{aligned} h(a, b) &= \frac{1}{a-b} \ln \frac{a}{b} , \\ g(a, b) &= \frac{1}{(a-b)^2} \left( 2 - \frac{a+b}{a-b} \ln \frac{a}{b} \right) . \end{aligned} \quad (19)$$

---

<sup>7</sup>Corrections associated with sbottom virtual loops are small if  $\tan \beta$  is small, and so they are not shown explicitly in eq. (15), although they were included in our numerical analysis.



Using these results, the full (numerically integrated) RG-improved value of  $m_{h^0}$  is reproduced to within an accuracy of about 2 GeV (assuming that supersymmetric particle masses lie below 2 TeV).

For  $|m_{\tilde{t}_1}^2 - m_{\tilde{t}_2}^2| \ll M_S^2$ , we may approximate  $g(a, a) \simeq -1/6a^2$  and  $h(a, a) \simeq 1/a$ . Then eq. (18) simplifies and takes the form

$$(\Delta m_{h^0}^2)_{\text{mix}} = \frac{g^2 N_c}{16\pi^2 m_W^2} m_t^4 \left\{ \frac{2X_t^2}{M_S^2} \left( 1 - \frac{X_t^2}{12M_S^2} \right) \right\}. \quad (20)$$

From eq. (20) it is easy to see that the maximal value of  $(\Delta m_{h^0}^2)_{\text{mix}}$ , and thus  $m_{h^0}$ , is achieved for  $|X_t| = \sqrt{6}M_S$ , which is sometimes called “maximal mixing”. For this value of  $|X_t|$ , the quantity in curly brackets in eq. (20) is equal to 6. For larger values of  $|X_t|$  this correction decreases, eventually turning negative. In the IFP scenario the approximation of nearly degenerate stops is not always applicable. (particularly for small values of  $|x|$  as shown in fig. 1), and one must include the stop mixing corrections in its full form [eq. (18)]. In the latter case,  $(\Delta m_{h^0}^2)_{\text{mix}}$  does not follow the simple behaviour discussed for the approximately mass-degenerate case; for example, values larger than 6 for the term in curly brackets in eq. (18) can result.

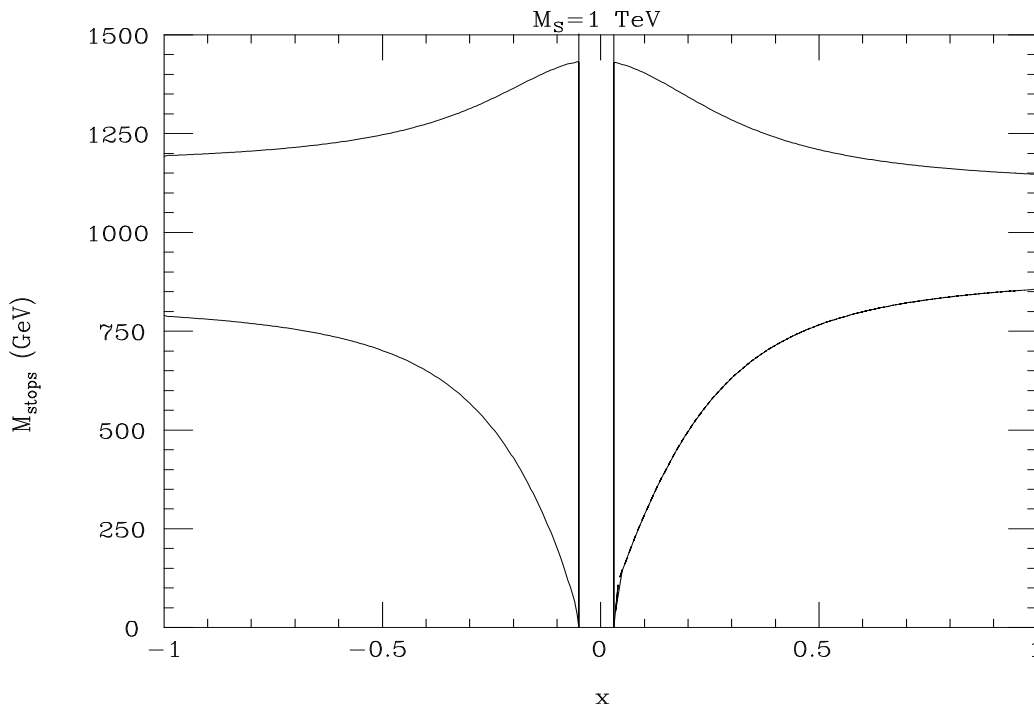


Figure 1: Stop mass eigenvalues,  $m_{\tilde{t}_1}$  (upper curves),  $m_{\tilde{t}_2}$  (lower curves), versus  $x = M/m$  in the IFP scenario for  $M_S = 1$  TeV. The indicated area around  $x = 0$  has one very light stop (or a negative value of  $m_{\tilde{t}_2}^2$ ) and is thus excluded experimentally.

As an example, one finds the following mass bounds for  $h^0$ , assuming  $M_t = 175$  GeV and  $M_S \lesssim 1$  TeV:  $m_{h^0} \lesssim 112$  GeV if stop mixing is negligible, while  $m_{h^0} \lesssim 125$  GeV if stop mixing is “maximal”. In both cases the upper bound corresponds to large  $\tan\beta$ .

When the IFP scenario is imposed, the parameter restrictions examined in Section 2 (*e.g.*, both  $\tan\beta$  and  $A_t$  are driven to fixed point values) imply that the Higgs mass upper limits quoted above are not saturated. Consequently the predicted value of  $m_{h^0}$  decreases substantially. In Section 4, we shall explore in detail the predictions for  $m_{h^0}$  in the IFP scenario as a function of the remaining free parameters.

## 4 Results

For the sake of definiteness and to facilitate the comparison with previous results in the literature, we first present detailed results for  $M_S = 1$  TeV. Subsequently, we will allow  $M_S$  to vary. It is then illustrative to start by showing the dependence of several relevant quantities as a function of the only remaining parameter,  $x \equiv M/m$ . In all the cases we will vary  $x$  over the range  $[-1, 1]$ , since for  $|x| \geq 1$  all the relevant quantities enter an asymptotic regime, as will be apparent from the figures. In addition, as explained at the end of Section 2, the values  $|x| \gtrsim 1$  are in conflict with CCB and UFB bounds.

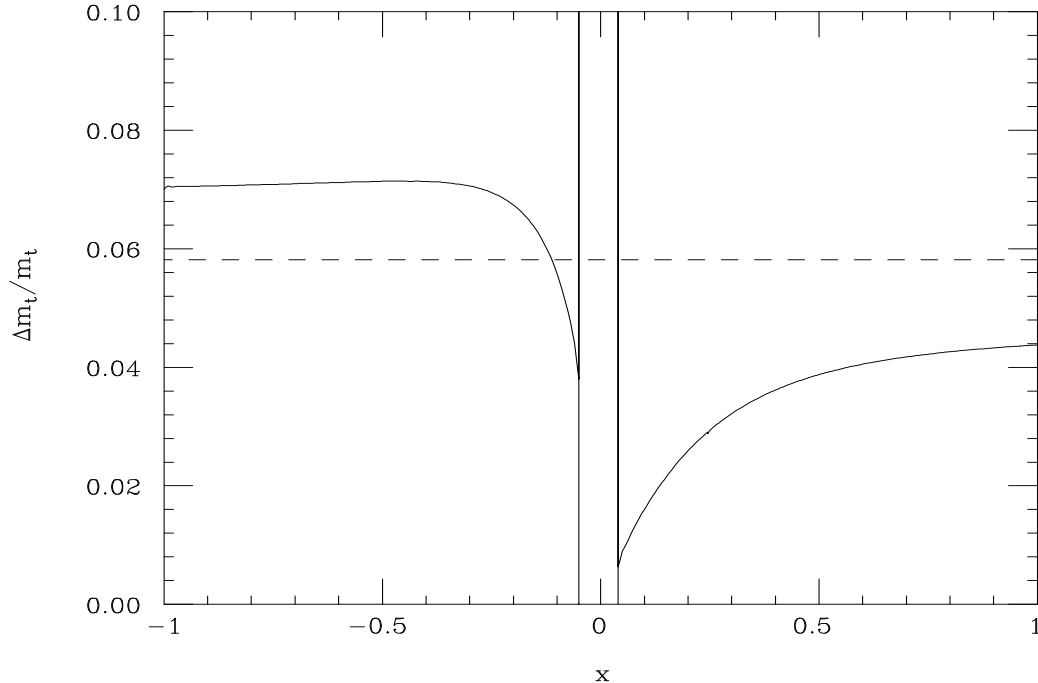


Figure 2: Stop/gluino threshold contribution [eq. (9)] to the relationship between the physical (pole) top-quark mass,  $M_t$ , and the  $\overline{\text{DR}}$  running mass,  $m_t \equiv m_t(M_t)$ , as a function of  $x \equiv M/m$  in the IFP scenario with  $M_S = 1$  TeV (solid line). For comparison, the gluon contribution [eq. (8)] is also exhibited (dashed line).

In fig. 1 we plot the two stop mass eigenvalues  $m_{\tilde{t}_1}, m_{\tilde{t}_2}$  vs.  $x$ . We note that for  $-0.07 \lesssim x \lesssim 0.03$  the mass of the lightest stop is lower than the present experimental bounds [40]. Thus, this region is excluded, as indicated in all figures shown in this

section. We also observe that eq. (20) is no longer a good approximation for  $(\Delta m_{h^0}^2)_{\text{mix}}$  when  $|x| \lesssim 0.4$ , and one must use eq. (18), as noted at the end of Section 3.

Fig. 2 shows the supersymmetric correction (due to stop/gluino loops) to the top-quark mass  $(\Delta m_t/m_t)_{\text{SUSY}}$  *vs.*  $x$ . Note that this correction is in general quite important. For comparison, we have also plotted the usual QCD correction,  $(\Delta m_t/m_t)_{\text{QCD}}$  (constant dashed line). Although the supersymmetric correction does not always have a definite sign in general models (as noted in Ref. [11]), this correction is always of the same sign as the QCD correction in the IFP scenario considered in this paper. This feature is a result of the constraints imposed on the stop and gluino masses. Moreover, the larger the positive value of  $\Delta m_t$ , the lower the value of  $\tan \beta$ . This can be seen from the dashed line in fig. 3, which shows the behavior of  $\tan \beta$  as a function of  $x$ .

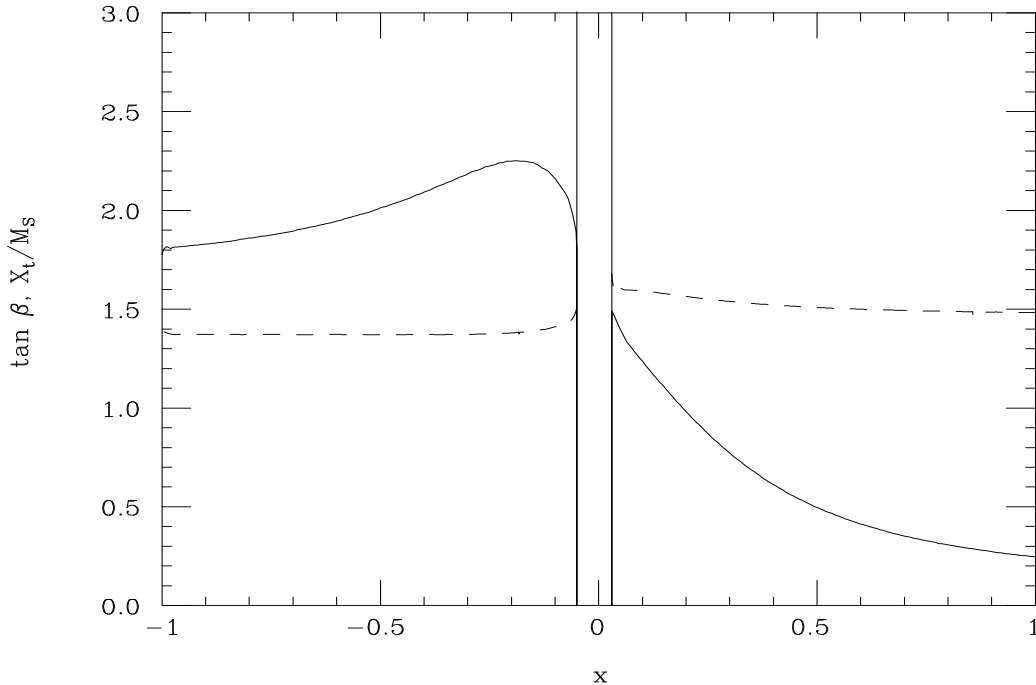


Figure 3: Predicted value of  $\tan \beta$  (dashed line) in the IFP scenario as a function of  $x \equiv M/m$  with  $M_S = 1$  TeV. The solid line depicts the stop mixing parameter  $X_t/M_S$  relevant for the determination of  $m_{h^0}$ .

Fig. 3 also shows the value of  $X_t/M_S$  as a function of  $x$ . Recall that both  $\tan \beta$  and  $X_t/M_S$  have a crucial impact on  $m_{h^0}$ . In particular (assuming that  $\tan \beta \geq 1$  and  $|X_t/M_S| \leq \sqrt{6}$ , which is always true in the IFP scenario considered here),  $m_{h^0}$  is an increasing function of both  $\tan \beta$  and  $|X_t/M_S|$ . However, as seen from fig. 3,  $\tan \beta$  and  $|X_t/M_S|$  do not attain their maximum values at the same value of  $x$ , which leads to an effective lowering of the maximum possible value of  $m_{h^0}$ . Moreover,  $X_t/M_S$  never reaches the “maximal value” of  $|X_t/M_S| = \sqrt{6}$ . This again limits the maximal value of  $m_{h^0}$  to lie below its MSSM upper bound.

The behavior of  $X_t/M_S$  shown in fig. 3 can be understood using eqs. (14) and (12) plus the expressions for  $\mu$ ,  $A_t$  and the third generation scalar squared-masses given in

Section 2 and the Appendix. In the limit where  $M_S \gg m_t$ , we obtain

$$\frac{X_t}{M_S} \simeq \frac{-1.2x + \cot\beta(\tan^2\beta - 1)^{-1/2}[(1 + 0.5\tan^2\beta) + (0.5 + 2\tan^2\beta)x^2]^{1/2}}{(0.25 + 2.75x^2)^{1/2}}. \quad (21)$$

For a typical value of  $\tan\beta$  (*e.g.*,  $\tan\beta \sim 1.5$  according to fig. 3), eq. (21) reaches a maximum at  $x \sim -0.2$  and lies below the “maximal value”  $|X_t/M_S| = \sqrt{6}$ .

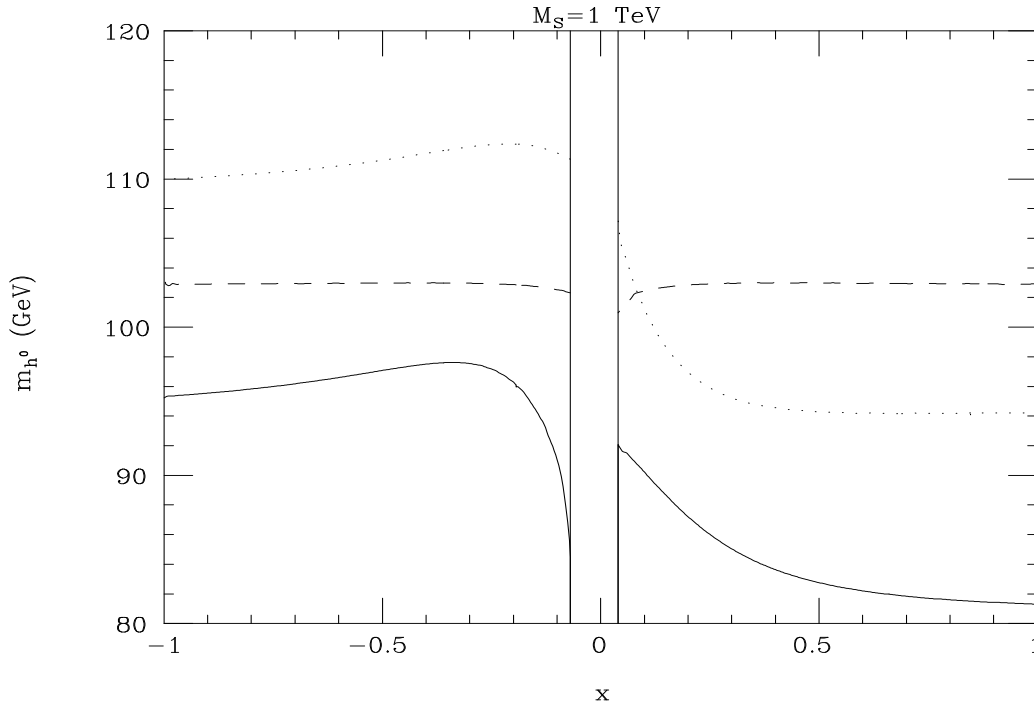


Figure 4: Different approximations to the lightest CP-even Higgs mass as a function of  $x \equiv M/m$  for the IFP scenario with  $M_S = 1$  TeV. The result of the calculation of this paper is given by the solid curve. If one omits the stop/gluino loop corrections to  $M_t/m_t(M_t)$  and assumes maximal stop mixing, one obtains the dashed curve. For comparison, the results of Ref. [7] are depicted by the dotted curve.

In fig. 4, the solid curve depicts the results for  $m_{h^0}$  in the IFP scenario considered in this paper. Note that the absolute upper bound on  $m_{h^0}$  corresponds to  $x \sim -0.3$ , although for  $x \lesssim -0.1$ , the variation of  $m_{h^0}$  with  $x$  is small. Numerically the bound on  $m_{h^0}$  reads  $m_{h^0} \leq 97$  GeV with an estimated error of  $\pm 2$  GeV (the quoted error is based on the results of Ref. [39]). In order to determine the impact on  $m_{h^0}$  of the new effects which we have incorporated in the calculation, and to compare with previous computations, we have included two additional curves in fig. 4. The dashed curve in fig. 4 is obtained by omitting the stop/gluino corrections to the physical (pole) top-quark mass,  $M_t$ , in terms of the  $\overline{\text{DR}}$  running mass  $m_t(M_t)$  [*i.e.*, taking  $(\Delta m_t/m_t)_{\text{SUSY}} = 0$ ], and setting the stop mixing parameter at its “maximal” value,  $|X_t/M_S| = \sqrt{6}$ . This procedure has been used in some works [36,37,38] to get an absolute upper bound on  $m_{h^0}$  in the IFP scenario, so the dashed curve reflects the

results of these papers. In addition, following Refs. [36,37], eq. (20) has been employed in obtaining the dashed curve for all values of  $x$ , although we know (see the discussion near the end of Section 3) that the underlying assumption of nearly degenerate stops is not appropriate for  $|x| \lesssim 0.3$ . (We note that the effects of non-degenerate stops were correctly taken into account in Ref. [38].) As anticipated, the simplifications which result in the dashed curve of fig. 4 lead to an overestimate of the  $m_{h^0}$  bound (over the full  $x$  range). Quantitatively, the overestimate is  $\sim 7$  GeV for  $x < 0$  and  $\sim 20$  GeV for  $x > 0$ . Finally, the dotted curve of fig. 4 corresponds roughly to the results of Ref. [7], which we include for the sake of comparison. The origin of the large discrepancy with our results is mainly due to two effects: (i) the omission of the supersymmetric corrections to  $(\Delta m_t/m_t)$ , and (ii) the use of a cruder method for the evaluation of  $m_{h^0}$ . There are also some minor differences related to the subtleties concerning the precise definition of  $\tan \beta$  and  $\mu$  at  $M_S$  (see Section 2), which have not been included in the dotted curve of fig. 4.

We conclude that previous results for  $m_{h^0}$  in the IFP scenario obtained in the literature have neglected a number of significant effects, which leads to a substantial reduction in the prediction of the upper bound for  $m_{h^0}$  as a function of the minimal SUGRA parameters. The Higgs mass upper bounds obtained previously are therefore too conservative. The more refined bound of  $m_{h^0} \lesssim 100$  GeV, obtained in this paper, is significant in that it lies within the reach of the LEP-2 Higgs search once the maximum LEP-2 energy and luminosity is achieved.

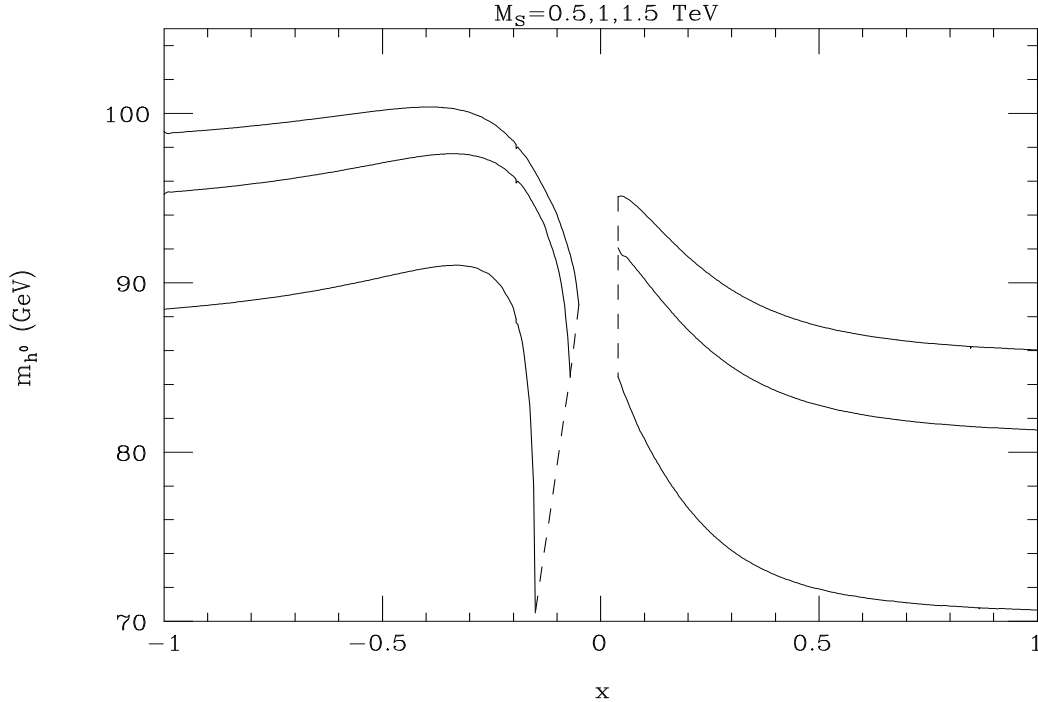


Figure 5: Lightest CP-even Higgs mass as a function of  $x \equiv M/m$  in the IFP scenario for different values of  $M_S = 0.5$  TeV (lower curve),  $M_S = 1$  TeV (middle curve) and  $1.5$  TeV (upper curve). For small  $x$ , the curves end on dashed lines where the stop mass lies below its experimental bound.

Finally, fig. 5 shows the value of  $m_{h^0}$  vs.  $x$  for different values of  $M_S$ ; curves for  $M_S = 0.5$  TeV, 1 TeV, and 1.5 TeV are shown. As expected, the predicted value of  $m_{h^0}$  increases logarithmically with  $M_S$ . Fig. 5 clearly shows a marked asymmetry in the predicted value of  $m_{h^0}$  under a change of sign of  $x$ . For  $x > 0$ , the stop mixing contribution to  $m_{h^0}$  is less important due to a destructive cancellation between  $A_t$  and  $\mu$  in  $X_t$  (see fig. 3). As a result,  $m_{h^0}$  is typically less than 90 GeV, which is almost excluded by the current LEP-2 limits on  $m_{h^0}$  [41]. For  $x < 0$ ,  $A_t$  and  $\mu$  have the same sign thereby enhancing  $X_t$ . The corresponding value of  $m_{h^0}$  is larger in this case, although for  $M_S \leq 1.5$  TeV, we still predict  $m_{h^0} \lesssim 100$  GeV. Larger values for  $M_S$  are less plausible, assuming that electroweak symmetry breaking is a natural consequence of low-energy supersymmetry. Hence, we conclude that the upper bound of the light CP-even Higgs mass is about 100 GeV, although the upper bound is not saturated in the IFP scenario over a significant region of the minimal SUGRA parameter space.

## 5 Conclusions

The quasi-infrared fixed point model is very attractive, since a number of quite general and well-motivated initial conditions lead to a highly predictive low-energy scenario. More precisely, working within the minimal SUGRA framework (with the assumption of universality of scalar and gaugino soft-supersymmetry-breaking masses), the only two independent parameters for low-energy physics are the common (high-energy) scalar ( $m$ ) and gaugino ( $M$ ) masses. We have studied in this framework the value of the light CP-even Higgs mass,  $m_{h^0}$ , which is a particularly relevant physical quantity since it turns out to be greatly constrained. We have taken into account some important effects that had not been previously considered. The most notable of these is the supersymmetric correction to the relation between the running and the physical top-quark masses, which lowers the value of  $\tan \beta$  and thus that of  $m_{h^0}$ . Other effects arise from the precise determination of the stop mixing parameter,  $X_t$  (which plays a major role in the computation of  $m_{h^0}$ ), as well as the observation that  $\tan \beta$  and  $X_t$  never conspire to raise  $m_{h^0}$  to its maximum possible value. In addition we have computed  $m_{h^0}$  using the most refined method available, including subdominant contributions and corrections from stop non-degeneracy. This substantially reduces the theoretical uncertainty of our results with respect to previous calculations in the literature.

Our predictions for  $m_{h^0}$  are significantly lower than previous evaluations, as illustrated in fig. 4. Fig. 5 displays our calculation of  $m_{h^0}$  and exhibits its dependence on  $x \simeq M/m$  for different values of  $M_S^2 \equiv \frac{1}{2}(m_{\tilde{t}_1}^2 + m_{\tilde{t}_2}^2)$ . For  $M_S \leq 1$  TeV we find  $m_{h^0} \leq 97 \pm 2$  GeV; the upper bound increases slightly for larger values of  $M_S$ . Since large values of  $M_S$  conflict with naturalness conditions associated with electroweak symmetry breaking, we conclude that  $m_{h^0} \lesssim 100$  GeV in the IFP scenario based on the constrained MSSM with universal scalar and gaugino mass parameters (as in minimal SUGRA and some superstring models), and the most plausible  $m_{h^0}$  values may be substantially smaller. These values of  $m_{h^0}$  are in the reach of the LEP-2 Higgs search, so the decisive test for the IFP scenario will soon be at hand.

## Acknowledgements

We thank B. de Carlos, R. Hempfling and C. Wagner for help and useful discussions.

## Appendix

Starting with universal scalar ( $m$ ) and gaugino ( $M$ ) soft masses at the unification scale  $M_X = [1.2 - 0.32t_s + 0.17t_s^2] \times 10^{16}$  GeV,<sup>8</sup> the soft masses at the supersymmetric scale [of order  $M_S$ , with  $t_s \equiv \ln(M_S/1 \text{ TeV})$ ] are:

$$m_{H_1}^2 = m^2 + 0.5M^2 \quad (22)$$

$$m_{H_2}^2 = m^2 + 0.5M^2 + \Delta m^2 \quad (23)$$

$$m_{L_i}^2 = m^2 + 0.5M^2 \quad (24)$$

$$m_{E_i}^2 = m^2 + 0.1M^2 \quad (25)$$

$$m_{Q_i}^2 = m^2 + [4.2 - 0.69t_s + 0.46t_s^2]M^2 + \frac{1}{3}\delta_{i3}\Delta m^2 \quad (26)$$

$$m_{U_i}^2 = m^2 + [3.8 - 0.69t_s + 0.46t_s^2]M^2 + \frac{2}{3}\delta_{i3}\Delta m^2 \quad (27)$$

$$m_{D_i}^2 = m^2 + [3.7 - 0.69t_s + 0.46t_s^2]M^2, \quad (28)$$

where the labels  $H_{1,2}$  are used for the soft masses of the Higgs doublets,  $L$  for the slepton doublets,  $E$  for the singlet sleptons,  $Q$  for the doublet squarks and  $U, D$  for up and down singlet squarks ( $i$  is a family index), and

$$\begin{aligned} \Delta m^2 = & -\frac{3}{2}m^2\frac{Y_t}{Y_f} + \left([1.6 - 0.19t_s + 0.1t_s^2]A_0M - \frac{1}{2}A_0^2\right)\frac{Y_t}{Y_f}\left(1 - \frac{Y_t}{Y_f}\right) \\ & + M^2\frac{Y_t}{Y_f}\left([1.3 - 0.34t_s + 0.1t_s^2]\frac{Y_t}{Y_f} - [3.8 - 0.69t_s + 0.6t_s^2]\right). \end{aligned} \quad (29)$$

In addition<sup>9</sup>,

$$\mu^2 = 1.8\mu_0^2\left(1 - \frac{Y_t}{Y_f}\right)^{1/2}, \quad (30)$$

$$B = B_0 - \frac{1}{2}A_0\frac{Y_t}{Y_f} - M\left(0.5 - [0.8 - 0.1t_s + 0.045t_s^2]\frac{Y_t}{Y_f}\right), \quad (31)$$

---

<sup>8</sup>This result exhibits the dependence of  $M_X$  on the supersymmetric scale  $M_S$ . The numerical coefficients of the prefactor are based on a fit to results obtained from a numerical integration of the two-loop RGEs, with  $\alpha(M_X) = 0.039$ .

<sup>9</sup>It may seem that eq. (30) is in conflict with eq. (11) in the quasi-infrared fixed point limit. Strictly speaking, we never reach this limit, so  $Y_t$  differs by a small amount from  $Y_f$ . Thus, in practice the low-energy value of  $\mu$  is obtained first from eq. (11), and then  $\mu_0$  is deduced from eq. (30). Clearly,  $\mu_0 \gg \mu$  for  $Y_t \simeq Y_f$ , which is equivalent to an unnatural fine-tuning in the electroweak symmetry breaking condition. Nevertheless, one can still be in the domain of the IFP solution without significantly violating the naturalness requirements.

$$A_t = A_0 \left( 1 - \frac{Y_t}{Y_f} \right) - M \left( [2.8 - 0.31t_s + 0.3t_s^2] - [1.6 - 0.2t_s + 0.09t_s^2] \frac{Y_t}{Y_f} \right). \quad (32)$$

In the above, the fitting of the numerical coefficients is accurate in the range  $500 \text{ GeV} \leq M_S \leq 1500 \text{ GeV}$ . Note that the values of the above parameters at  $M_S$  (particularly those whose running is affected by  $\alpha_s$ , such as the squark squared-mass parameters and  $A_t$ ) are substantially different from the corresponding values at  $m_Z$  (see Ref. [7]).

## References

- [1] S. Dimopoulos and H. Georgi, *Nucl. Phys.* **B193** (1981) 150; H. Georgi, *Phys. Lett.* **169B** (1986) 231; L.J. Hall, V.A. Kosteletsky, and S. Raby *Nucl. Phys.* **B267** (1986) 415.
- [2] H.P. Nilles, *Phys. Rep.* **110** (1984) 1.
- [3] B. de Carlos, J.A. Casas and C. Muñoz, *Phys. Lett.* **B299** (1993) 234; V. Kaplunovsky and J. Louis, *Phys. Lett.* **B306** (1993) 269; A. Brignole, L. E. Ibáñez and C. Muñoz, *Nucl. Phys.* **B422** (1994) 125; J. A. Casas, *Phys. Lett.* **B384** (1996) 103.
- [4] C.T. Hill, *Phys. Rev.* **D24** (1981) 691; C.T. Hill, C.N. Leung, and S. Rao, *Nucl. Phys.* **B262** (1985) 517.
- [5] L. Ibáñez and C. López, *Nucl. Phys.* **B233** (1984) 511.
- [6] V. Barger, M. S. Berger, P. Ohmann and R. J. N. Phillips, *Phys. Lett.* **B314** (1993) 351.
- [7] M. Carena, M. Olechowski, S. Pokorski and C.E.M. Wagner, *Nucl. Phys.* **B419** (1994) 213; M. Carena and C.E.M. Wagner, *Nucl. Phys.* **B452** (1995) 45.
- [8] M. Lanzagorta and G.G. Ross, *Phys. Lett.* **B349** (1995) 319.
- [9] B. Schrempp and M. Wimmer, *Prog. Part. Nucl. Phys.* **37** (1996) 1.
- [10] P. Langacker and N. Polonsky, *Phys. Rev.* **D50** (1994) 2199.
- [11] J. Feng, N. Polonsky and S. Thomas, *Phys. Lett.* **B370** (1996) 95; N. Polonsky, *Phys. Rev.* **D54** (1996) 4537.
- [12] P. Chankowski and S. Pokorski, CERN-TH-97-28 [hep-ph/9702431], to appear in *Perspectives on Higgs Physics II*, edited by G.L. Kane (World Scientific, Singapore, 1998).
- [13] B. Brahmachari, *Mod. Phys. Lett.* **A12** (1997) 1969.
- [14] S. Abel and B. Allanach, [hep-ph/9707436].
- [15] B. Pendleton and G.G. Ross, *Phys. Lett.* **98B** (1981) 291.



- [16] A.E. Nelson and L. Randall, *Phys. Lett.* **B316** (1993) 516; R. Rattazzi and U. Sarid, *Phys. Rev.* **D53** (1996) 1553.
- [17] P.M. Ferreira, I. Jack and D.R.T. Jones, *Phys. Lett.* **B392** (1997) 376.
- [18] D. Pierce, hep-ph/9407202; J.A. Bagger, K. Matchev and D.M. Pierce, *Phys. Lett.* **B348** (1995) 443; J.A. Bagger, K. Matchev, D.M. Pierce and R. Zhang, *Nucl. Phys.* **B491** (1997) 3.
- [19] B.D. Wright, hep-ph/9404217; A. Donini, *Nucl. Phys.* **B467** (1996) 3.
- [20] N. Gray, D.J. Broadhurst, W. Grafe and K. Schilcher, *Z. Phys.* **C48** (1990) 673.
- [21] R. Hempfling and B.A. Kniehl, *Phys. Rev.* **D51** (1995) 1386.
- [22] T. Kobayashi and Y. Yamagishi, *Phys. Lett.* **B381** (1996) 169.
- [23] G. Gamberini, G. Ridolfi and F. Zwirner, *Nucl. Phys.* **B331** (1990) 331; R. Arnowitt, P. Nath, *Phys. Rev.* **D46** (1992) 3981.
- [24] B. de Carlos and J.A. Casas, *Phys. Lett.* **B309** (1993) 320.
- [25] H.E. Haber, in *Supersymmetry Part I (Theory)*, in the Particle Data Group mini-review, 1997 off-year partial update for the 1998 edition (URL: <http://pdg.lbl.gov/>)
- [26] J.M. Frere, D.R.T. Jones and S. Raby, *Nucl. Phys.* **B222** (1983) 11; L. Alvarez-Gaumé, J. Polchinski and M. Wise, *Nucl. Phys.* **B221** (1983) 495; J.P. Derendinger and C.A. Savoy, *Nucl. Phys.* **B237** (1984) 307; C. Kounnas, A.B. Lahanas, D.V. Nanopoulos and M. Quirós, *Nucl. Phys.* **B236** (1984) 438; J.F. Gunion, H.E. Haber and M. Sher, *Nucl. Phys.* **B306** (1988) 1; A. Kusenko, P. Langacker and G. Segre, *Phys. Rev.* **D54** (1996) 5824.
- [27] J.A. Casas, C. Muñoz and A. Lleyda, *Nucl. Phys.* **B471** (1996) 3.
- [28] J.A. Casas, A. Lleyda and C. Muñoz, *Phys. Lett.* **B389** (1996) 305.
- [29] M. Carena, P.M. Zerwas *et al.*, in *Physics at LEP2*, Volume 1, edited by G. Altarelli, T. Sjöstrand and F. Zwirner, CERN Yellow Report 96-01 (1996) pp. 351–462.
- [30] H.E. Haber and R. Hempfling, *Phys. Rev. Lett.* **66** (1991) 1815; Y. Okada, M. Yamaguchi and T. Yanagida, *Prog. Theor. Phys.* **85** (1991) 1 ; J. Ellis, G. Ridolfi and F. Zwirner, *Phys. Lett.* **B257** (1991) 83 ; **B262** (1991) 477.
- [31] R. Barbieri and M. Frigeni, *Phys. Lett.* **B258** (1991) 395; M. Drees and M.M. Nojiri, *Phys. Rev.* **D45** (1992) 2482.
- [32] R. Hempfling and A.H. Hoang, *Phys. Lett.* **B331** (1994) 99.

- [33] P.H. Chankowski, S. Pokorski and J. Rosiek, *Phys. Lett.* **B274** (1992) 191; *Nucl. Phys.* **B423** (1994) 437 ; A. Brignole, *Phys. Lett.* **B281** (1992) 284; A. Yamada, *Phys. Lett.* **B263** (1991) 233 ; *Z. Phys.* **C61** (1994) 247; A. Dabelstein, *Z. Phys.* **C67** (1995) 495; D.M. Pierce, J.A. Bagger, K. Matchev and R. Zhang, *Nucl. Phys.* **B491** (1997) 3.
- [34] R. Barbieri, M. Frigeni and F. Caravaglios, *Phys. Lett.* **B258** (1991) 167; Y. Okada, M. Yamaguchi and T. Yanagida, *Phys. Lett.* **B262** (1991) 54; D.M. Pierce, A. Papadopoulos and S. Johnson, *Phys. Rev. Lett.* **68** (1992) 3678; K. Sasaki, M. Carena and C.E.M. Wagner, *Nucl. Phys.* **B381** (1992) 66; H.E. Haber and R. Hempfling, *Phys. Rev.* **D48** (1993) 4280; J. Kodaira, Y. Yasui and K. Sasaki, *Phys. Rev.* **D50** (1994) 7035.
- [35] J.R. Espinosa and M. Quirós, *Phys. Lett.* **B266** (1991) 389.
- [36] J.A. Casas, J.R. Espinosa, M. Quirós and A. Riotto, *Nucl. Phys.* **B436** (1995) 3.
- [37] M. Carena, J.R. Espinosa, M. Quirós and C.E.M. Wagner, *Phys. Lett.* **B355** (1995) 209.
- [38] M. Carena, M. Quirós and C.E.M. Wagner, *Nucl. Phys.* **B461** (1996) 407.
- [39] H.E. Haber, R. Hempfling and A.H. Hoang, *Z. Phys.* **C75** (1997) 539.
- [40] M. Schmitt, in *Supersymmetry Part II (Experiment)*, in the Particle Data Group mini-review, 1997 off-year partial update for the 1998 edition (URL: <http://pdg.lbl.gov/>)
- [41] A. Sopczak, Karlsruhe preprint IEKP-KA-97-14 (1997) [hep-ph/9712283].